

# Inhibition of the Main Protease 3CL<sup>Pro</sup> of the Coronavirus Disease 19 via Structure-Based Ligand Design and Molecular Modeling.

Marina Macchiagodena, Marco Pagliai, and Piero Procacci\*

*Dipartimento di Chimica "Ugo Schiff", Universit  degli Studi di Firenze, Via della  
Lastruccia 3, Sesto Fiorentino, I-50019 Italy*

E-mail: procacci@unifi.it

## Abstract

We have applied a computational strategy, based on the synergy of virtual screening, docking and molecular dynamics techniques, aimed at identifying possible lead compounds for the non-covalent inhibition of the main protease 3CL<sup>Pro</sup> of the SARS-Cov2 Coronavirus. Based on the recently resolved 6LU7 PDB structure, ligands were generated using a multimodal structure-based design and then optimally docked to the 6LU7 monomer. Docking calculations show that ligand-binding is strikingly similar in SARS-CoV and SARS-CoV2 main proteases, irrespectively of the protonation state of the catalytic CYS-HIS dyad. The most potent docked ligands are found to share a common binding pattern with aromatic moieties connected by rotatable bonds in a pseudo-linear arrangement. Molecular dynamics calculations fully confirm the stability in the 3CL<sup>Pro</sup> binding pocket of most potent binder identified by docking, namely a chlorophenyl-pyridyl-carboxamide derivative.

At the beginning of this year, the world was dismayed by the outbreak of a new severe viral acute respiratory syndrome (SARS), currently known as COVID-19, that rapidly spreads

from its origin in the Hubei Chinese district to virtually whole China and, as of today, to more than twenty nations in five continents.<sup>1</sup> The new coronavirus, named SARS-CoV2 and believed to have a zoonotic origin from the “wet markets” of the Chinese city Wuhan, has infected thus far about 80000 people worldwide with nearly 13000 in critical conditions, causing the death of more than 2000 people. SARS-CoV2 belongs to the family of the Coronaviridae and, as such, its genome<sup>2,3</sup> has a large identity, from 80% to 96%,<sup>4</sup> with that of the SARS-CoV whose epidemic started in early in 2003 and ended in the summer of the same year.

Most of the Coronaviridae genome encodes two large polyproteins, pp1a and, through ribosomal frameshifting during translation,<sup>5</sup> pp1ab. These polyproteins are cleaved and transformed in mature non-structural proteins (NSPs) by the two proteases 3CL<sup>pro</sup> (3C-like protease) and PL<sup>pro</sup> (Papain Like Protease) encoded by the open reading frame 1.<sup>6</sup> NSPs, in turn, play a fundamental role in the transcription/replication during the infection.<sup>5</sup> Targeting these proteases may hence constitute a valid approach for antiviral drug design. The cysteine protease 3CL<sup>pro</sup>, in particular, is responsible for the cleavage of at least 11 sites during proteolytic processing of polyproteins pp1a and pp1ab. Cleavage occurs at the glutamine residue in the P1 position of the substrate via the protease CYS-HIS dyad in which the cysteine thiol functions as the nucleophile in the proteolytic process.<sup>7</sup> The catalytically active 3CL<sup>pro</sup> is a dimer. While dimerization is believed to provide a substrate-binding cleft between the two monomers,<sup>8</sup> in the dimer the solvent-exposed CYS-HYS dyads are symmetrically located at the opposite edges the cleft, probably acting independently.<sup>9</sup> As no host-cell proteases are currently known with this specificity, early drug discovery was directed towards the so-called covalent Michael inhibitors,<sup>10</sup> via electrophilic attack to the cysteinate of the 3CL<sup>pro</sup> dyad. On the other hand, the consensus in drug discovery leads to excluding electrophiles from drug candidates for reasons primarily relating to safety and adverse effects such as allergies, tissue destruction, or carcinogenesis.<sup>11</sup>

In spite of the initial effort in developing small-molecule compounds (SMC) with anti-

coronavirus activity immediately after the SARS outbreak,<sup>12</sup> no anti-viral drug was ever approved or even reached the clinical stage due to a sharp decline in funding of coronavirus research after 2005-2006, based on the patently erroneous conviction by policy-makers and scientists that chance of a repetition of a new zoonotic transmission was extremely unlikely. The most potent non-covalent inhibitor for 3CL<sup>pro</sup>, ML188, was actually reported nearly ten years ago<sup>13</sup> with moderate activity in the low micromolar range.<sup>14</sup> Development of SMC targeting 3CL<sup>pro</sup> can hence be restarted from SARS experience, by exploiting the large level of homology between SARS-CoV and SARS-CoV2 3CL<sup>pro</sup>. According to the latest report of the structure of 3CL<sup>pro</sup> from SARS-CoV2<sup>15</sup> (PDB code 6LU7) and the available structure of 3CL<sup>pro</sup> from SARS-CoV,<sup>12</sup> (PDB code 1UK4), the two main proteases differ by only 12 amino acids, with  $\alpha$  carbon atoms all lying at least 1 nm away from the 3CL<sup>pro</sup> active site (see Figure 1a). The substrate-binding pockets (shown as a surface representation) of two

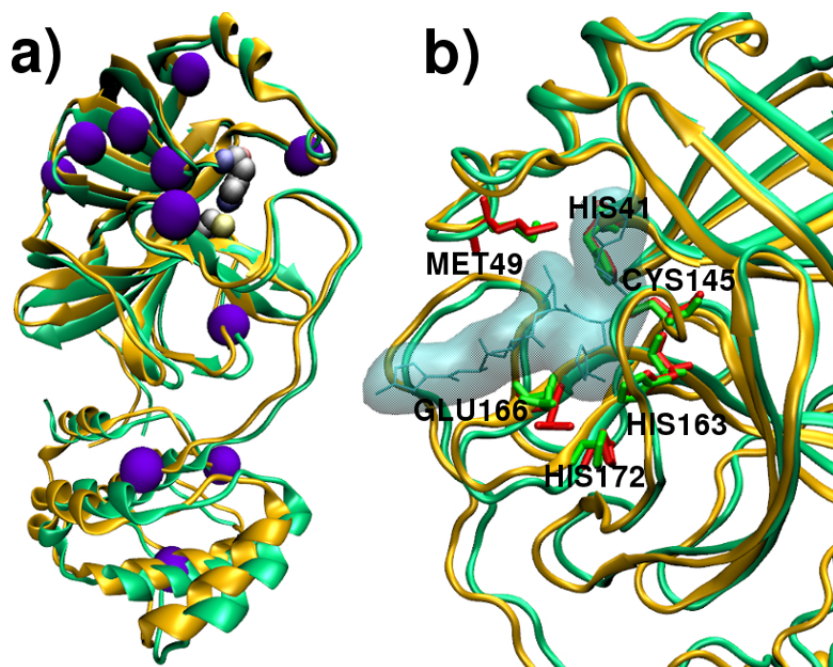


Figure 1: a):SARS-CoV2(orange, pdbcode 6LU7) and SARS-CoV (green, pdbcode 1UK4) main proteases. Violet spheres corresponds to the alpha carbons of the 12 differing residues in the two structures. Grey spheres indicate the CYS-HIS dyad b): Highlighted view of the binding pocket with the main residues in bond representation (green and red for SARS-CoV2 and SARS-CoV, respectively). The shaded region mark the binding site for the substrate (N3 compound in 6LU7 structure)

coronavirus main proteases are compared in Figure 1b, exhibiting a strikingly high level of alignment of the key residues involved in substrate binding, including the CYS145···HIS41 dyad, and HIS163/HIS172. The latter residues, along with GLU166, are believed to provide the opening gate for the substrate in the active state of the protomer.<sup>12</sup>

Figure 1(a,b) strongly suggest that effective non-covalent inhibitors for SARS-CoV and SARS-CoV2 main proteases should share the same structural and chemical features. In order to investigate this matter, we have performed a molecular modeling study on both the 6LU7 and 1UK4 PDB structures using a molecular docking approach. 6LU7 is the monomer of the main protease in the active state with the N3 peptidomimetic inhibitor<sup>15</sup> while 1UK4 is the dimer with the protomer chain A in the active state.<sup>12</sup> The main protease monomer contains three domains. Domains I and II (residues 8-101 and residues 102-184) are made of antiparallel  $\beta$ -barrel structures in a chymotrypsin-like fold responsible for catalysis. The substrate-binding site is located in a cleft between these two domains.<sup>16</sup>

The 6LU7 structure was first fed to the *PlayMolecule* web application by Acellera<sup>17</sup> ([www.playmolecule.org](http://www.playmolecule.org)) using a novel and effective virtual screening technique for the multimodal structure-based ligand design,<sup>18</sup> called Ligand Generative Adversarial Network (LIGANN). Ligands in LIGANN are generated so as to match the shape and chemical attributes of the binding pocket and decoded into a sequence of SMILES enabling directly the structure-based *de novo* drug design. SMILES code for optimally shaped ligands were obtained using the default LIGANN values for shapes and channels with the cubic box center set at the midpoint vector connecting the SH and NE atoms of the CYS-HIS dyad in the 6LU7 crystallographic structure of SARS-CoV2 main protease monomer in the active state. The *PlayMolecule* interface delivered 93 optimally fit non-congeneric compounds, spanning a significant portion of the chemical space, whose SMILES and structures are reported in the Supporting Information. Each of these compounds was docked to the 6LU7 and to the 1UK4 (monomer, chain A) structures, using Autodock4.<sup>19</sup> For both structures, the docking was repeated by setting the dyad with the residue in their neutral (CYS-HIS) and charged state

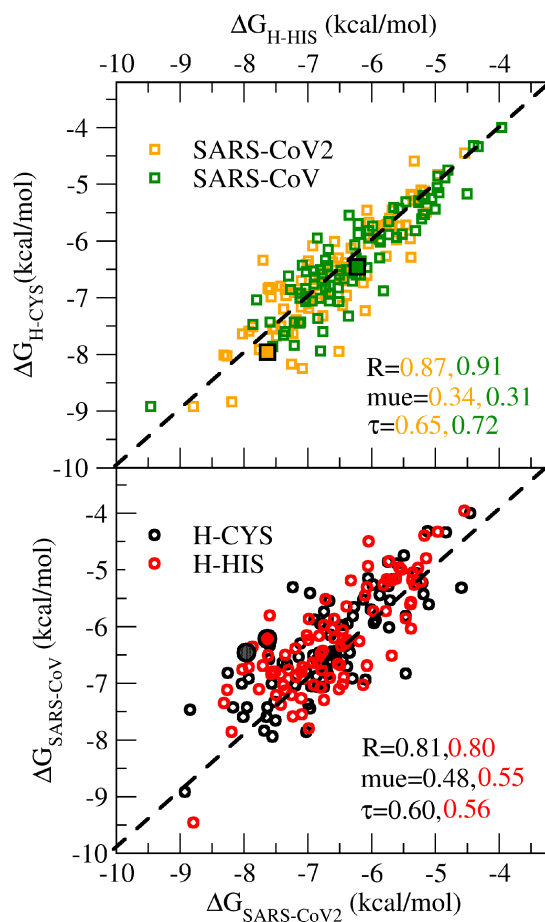


Figure 2: Correlation diagrams of autodock-computed binding free energies for 93 ligands of the SARS-CoV and SARS-CoV2 3CL<sup>pro</sup> structures.  $R$ ,  $\text{mue}$ ,  $\tau$  indicate the Pearson correlation coefficient, the mean unsigned error, and the Kendall rank coefficient, respectively. Upper panel: correlation diagram between ligand free energies obtained with the charged  $\text{CYS}^{-1}\text{-HIS}^+$  (x-axis) and with neutral CYS-HIS (y-axis) dyad. Lower panel: correlation diagram between ligand free energies of SARS-CoV2 and SARS-CoV.

(CYS<sup>-</sup>/HIS<sup>+</sup>). The searching box for optimal docking was again approximately centered at the CYS-HIS dyad and full ligand flexibility was assumed. The minimum search was done using 50 cycles of Lamarckian Genetic Algorithm and empirical free energy scoring function with Babel-generated<sup>20</sup> Gesteiger atomic charges. Further details on Docking parameters are given in the Supporting Information.

Results for the binding free energies of the 93 LIGGAN-determined 3CL<sup>pro</sup> ligands are reported in Figure 2. Binding free energies are comprised in the range 4-9 kcal/mol and are found to be strongly correlated for the two protonation states of the CYS-HIS dyad, hence indicating a weak dependency of the inhibition potency on pH in the range 6-8. Correlation is still quite high when ligand binding free energies for the main proteases are compared, confirming that good binders for SARS-CoV are, in general, also good binders for SARS-CoV2 3CL<sup>pro</sup>.

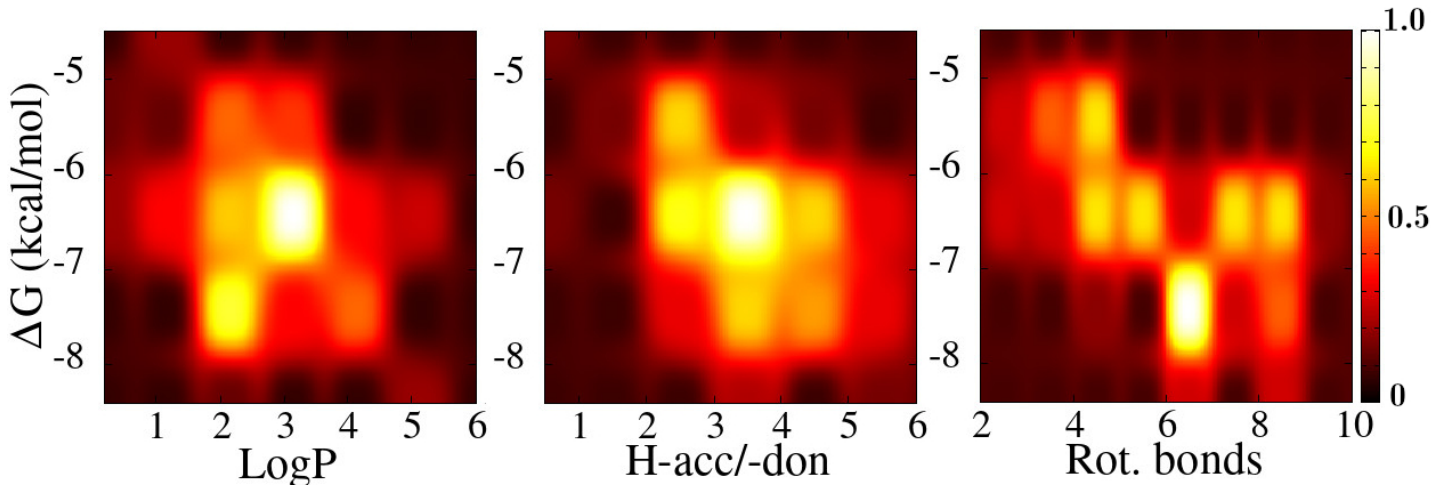


Figure 3: 2D probability histograms  $\Delta G$  with LogP (left), Hbond acceptors or donors (center) and rotatable bonds (right) for the LIGGAN-determined compounds of Table 1 of the Supporting Information. The common color-coded  $z$ -scale on the right corresponds to the 2D probability.

For each of these compounds, using the knowledge-based XLOGP3 methodology,<sup>21</sup> we computed the octanol/water partition coefficient (LogP) to assess the distribution in hydrophobic and cytosolic environments. Computed LogP values range from -0.5 to a max-

imum of 5 with a number of rotatable bonds from 2 to a maximum of 12. Most of the LIGGAN compounds bear from 2 to 5 H-bond acceptor or donors. Values of  $\Delta G$  and LogP for each of the 93 compounds are reported in Table 1 of the Supporting Information. In Figure 3 we show the 2D probability distributions for  $\Delta G$  correlated in turn to the LogP, number of H-bond donor/acceptors and number of rotatable bonds. We note, on the left and central panel, sharp maxima for LogP = 3 : 4,  $\Delta G = -7 : -8$  and for H-acc/don = 3,  $\Delta G = -6 : -7$ , respectively, suggestive of a ligand-protein association driven mostly by hydrophobic interactions. We must stress here that the computed  $\Delta G$  pertains to the associations of the ligand with *one* protein whatever the state of association of the protein. At free ligand concentration equal to  $K_d \equiv e^{-\Delta G/RT}$ , i.e. when half of the protein molecules are inhibited, the probability to have *both* monomers inhibited is equal to 1/4, whatever the dissociation constant of the dimer,<sup>22</sup> hence the need for identifying nanomolar or subnanomolar inhibitors of 3CL<sup>pro</sup>.

Figure 4 shows the chemical structures of the five compounds exhibiting the highest binding affinity to the 6LU7 main protease of SARS-CoV2 when the CYS-HIS dyad is in the neutral state. None of these compounds is commercially available, although some of them (**27**, **31**, **40**) show a high degree of similarity with known structures according to the Tanimoto metrics.<sup>23</sup> The LIGGAN-determined structures of Figure 4, as well as many of those reported in Figures 1-5 of the Supporting Information, seem to share a common pattern with aromatic moieties connected by rotatable bonds in a pseudo-linear arrangement. In Table 1, the binding free energy data of these five best ligands are shown for both CoV proteases and both protonation states of the catalytic dyad. As previously inferred based on 3CL<sup>pro</sup> similarities (see Figure 1), inspection of Table 1 confirms that SARS-CoV2 best binders **27**, **29**, **39**, **77**, **19** are also good binders for SARS-CoV 3CL<sup>pro</sup>. Remarkably, compound **27** is consistently the most potent ligand for the two proteases, irrespectively of the dyad protonation state. In the Table 1 we also report the Autodock4-computed binding free energy for ML188. The Autodock4-predicted binding free energy for the association of ML188-SARS-

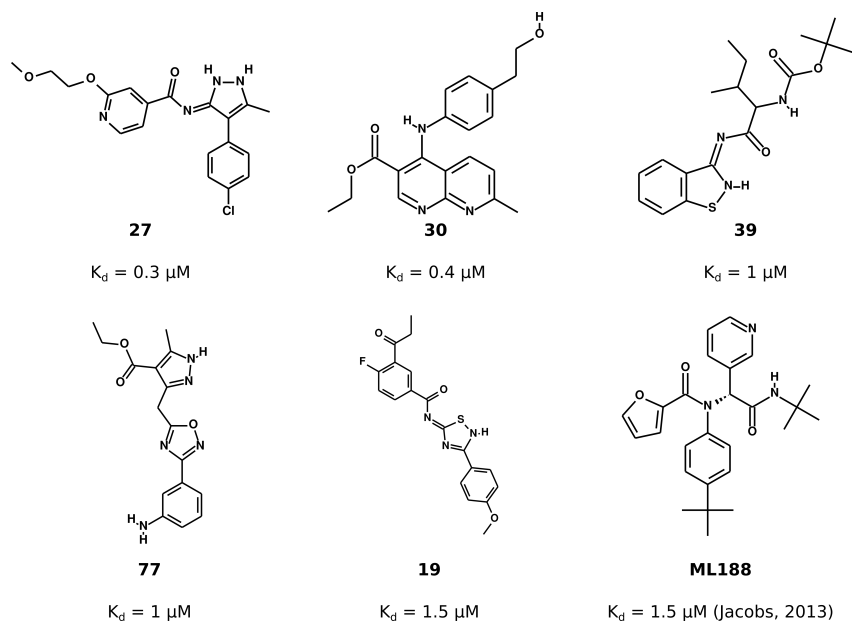


Figure 4: fig:best binders for SARS-CoV2 main protease

Cov protease is -6.2 and -6.5 kcal/mol for the H-HIS and H-CYS tautomers, not too distant indeed from the experimentally determined value of -8 kcal/mol, hence lending support for the LIGGAN-Autodock4 protocol used in identifying the lead compounds of Table 1.

Table 1: Computed binding free energies (kcal/mol),  $\Delta G$ , of the best five binders (see the full list in the Supporting information) for SARS-CoV2 3CL<sup>PRO</sup>.  $\Delta G$  values are reported for the two protonation state of the dyad and for SARS-Cov and SARS-Cov2 main protease.

Comp.	CoV19		SARS		LogP
	H-CYS	H-HIS	H-CYS	H-HIS	
27	-8.92	-8.79	-8.92	-9.46	4.90
30	-8.84	-8.19	-7.47	-7.86	3.74
39	-8.25	-7.08	-6.82	-6.72	6.06
77	-8.17	-7.25	-7.43	-7.21	2.03
19	-8.03	-8.26	-7.01	-7.12	5.58
ML188	-7.96	7.63	6.46	6.22 <sup>a</sup>	4.97

<sup>a</sup>Experimental value for ML188 is<sup>14</sup>  $\Delta G = -7.98$  kcal/mol.

In order to assess the stability of the 3CL<sup>PRO</sup>-**27** association, we have performed extensive molecular dynamics simulations of the ligand-protein bound state with explicit solvent, using the GROMACS program.<sup>2,3</sup> The overall structural information was obtained by combining data from three independent simulations (for a total of about 120 ns), all started from

the best docking pose of **27** on the 6LU7 monomeric structure with a different seed for initial velocity randomization. These simulations are performed following a state-of-the-art technical protocol extensively described in Ref.<sup>26</sup> Further methodological aspects are provided in the Supporting Information. In Figure 5, we show the probability distribution,

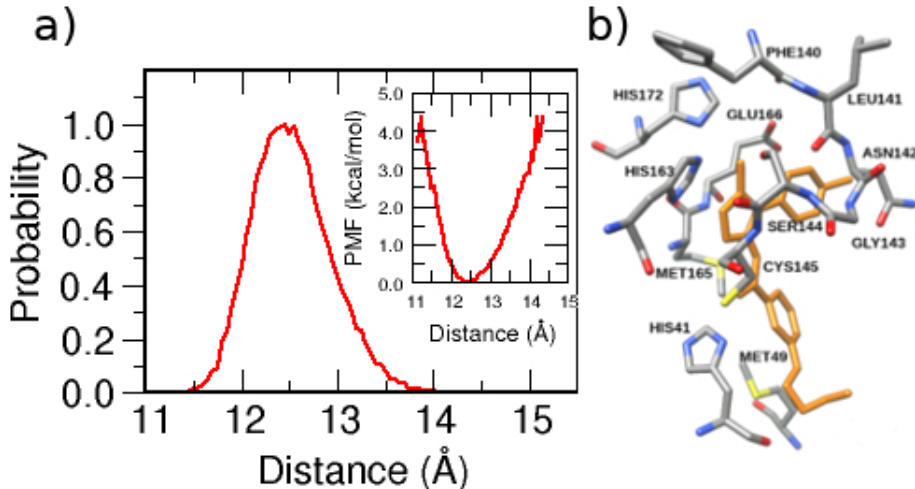


Figure 5: a) Probability distribution of the distance between the centers of mass of compound **27** and domain I+II of 3CL<sup>PRO</sup> as obtained from triplicates MD simulations (120 ns in total) (in the inset the corresponding PMF is shown). b) Binding pocket of 6LU7 with ligand **27**. Time record of the minimal distances between ligand and the depicted nearby residues are reported in Figures 6, 7 of the Supporting Information.

$P(R)$ , of the distance  $R$  between the center of mass (CoM) of the ligand and that of the domains I+II of 3CL<sup>PRO</sup>. The distribution has nearly a Gaussian shape with a half-width of about 1 Å, exhibiting only a minor positive skewness and defining a tight binding site volume  $V_{\text{site}}$  of few Å<sup>3</sup> at most.<sup>27</sup> The MD-determined  $P(R)$  neatly shows that the ligand never leaves the binding pocket of the chymotrypsin-like fold at any stage during the whole simulation. In the inset of Figure 5a we show the potential of mean force (PMF) along the intermolecular ligand-protein CoM distance  $R$ , computed as  $v(R) = -RT \log(P(R)/\max[P(r)])$ . As  $1/K_d = \int_{V_{\text{site}}} e^{-\beta v(R)} d\mathbf{R}$ ,<sup>28</sup> the steepness of the curve is suggestive of a profound minimum with respect to the zero in the bulk at large  $R$  and hence of a large association constant, fully confirming the indication obtained from the Docking calculations. In Figure 5b we show all polar and hydrophobic residues found in at least 90% of the simulation time within 4.5

and 5.5 Å distance, respectively, from any atom of the ligand **27**. Basically all putative essential residues for binding (see Figure 1) are included, with the important addition of Met165, Phe140 and Leu141 hydrophobic residues that consistently linger near the pyrazolic or the chlorinated phenyl rings of **27**, in agreement with the hydrophobic character of the interaction.

To the light of these encouraging preliminary results, in the near future, in order to single out the optimal lead compound for 3CL<sup>pro</sup> inhibition, we are planning to perform absolute binding free energies on the most potent LIGGAN-Autodock4 binders using fast switching double annihilation non-equilibrium technique as described in Ref.<sup>29,30</sup> On the other hand, Figures 3 and 5 shows possible avenues for improvement. For example, forcing the L-shaped binding structure (see Figure 5b) in bulk also, possibly by redesigning the rotatable connectors in the ligand, may reduce the penalty due conformational entropy loss upon binding,<sup>27</sup> hence boosting the ligand affinity for 3CL<sup>pro</sup>. Building upon this knowledge, we hence plan to optimize the lead using MD simulations coupled to efficient relative binding free energy calculation via free energy perturbation on congeneric variants,<sup>31</sup> eventually providing *in silico* determined anti-viral compounds to be synthesized and experimentally tested *in vitro* and *in vivo*.

We finally note that the infection rate for COVID-19 is currently declining for days. As the road for delivering an effective anti-viral drug is still a long one indeed, the SARS-Cov2 harsh lesson, nonetheless, should not be forgotten once the emergency will end, hoping that our contribution can pave the way for the design of effective non-covalent antiviral drugs for the present and future Coronavirus emergencies.

## References

- (1) Dong, E.; Du, H.; Gardner, L. An Interactive Web-Based Dashboard to Track COVID-19 in Real Time. *Lancet Infect. Dis.* **2020**,

- (2) 2020; Viralzone News, <https://viralzone.expasy.org>.
- (3) 2020; The National Center for Biotechnology Information, <https://www.ncbi.nlm.nih.gov>.
- (4) Shanker, A.; Bhanu, D.; Alluri, A. Analysis of Whole Genome Sequences and Homology Modelling of a 3C Like Peptidase and a Non-Structural Protein of the Novel Coronavirus COVID-19 Shows Protein Ligand Interaction with an Aza-Peptide and a Noncovalent Lead Inhibitor with Possible Antiviral Properties. *ChemRxiv* **2020**,
- (5) Thiel, V.; Ivanov, K. A.; Putics, A.; Hertzog, T.; Schelle, B.; Bayer, S.; Weißbrich, B.; Snijder, E. J.; Rabenau, H.; Doerr, H. W.; Gorbalenya, A. E.; Ziebuhr, J. Mechanisms and Enzymes Involved in SARS Coronavirus Genome Expression. *J. Gen. Virol.* **2003**, *84*, 2305–2315.
- (6) Hilgenfeld, R. From SARS to MERS: Crystallographic Studies on Coronaviral Proteases Enable Antiviral Drug Design. *FEBS J.* **2014**, *281*, 4085–4096.
- (7) Anand, K.; Ziebuhr, J.; Wadhwani, P.; Mesters, J. R.; Hilgenfeld, R. Coronavirus Main Proteinase (3CLpro) Structure: Basis for Design of Anti-SARS Drugs. *Science* **2003**, *300*, 1763–1767.
- (8) Chuck, C.-P.; Chong, L.-T.; Chen, C.; Chow, H.-F.; Wan, D. C.-C.; Wong, K.-B. Profiling of Substrate Specificity of SARS-CoV 3CL. *PloS One* **2010**, *5*, e13197–e13197.
- (9) Shi, J.; Sivaraman, J.; Song, J. Mechanism for Controlling the Dimer-Monomer Switch and Coupling Dimerization to Catalysis of the Severe Acute Respiratory Syndrome Coronavirus 3C-Like Protease. *J. Virol.* **2008**, *82*, 4620–4629.
- (10) Johansson, M. H. Reversible Michael Additions: Covalent Inhibitors and Prodrugs. *Mini-Rev. Med. Chem.* **2012**, *12*, 1330–1344.

- (11) Vasudevan, A.; Argiriadi, M. A.; Baranczak, A.; Friedman, M. M.; Gavriilyuk, J.; Hobson, A. D.; Hulce, J. J.; Osman, S.; Wilson, N. S. In *Chapter One - Covalent Binders in Drug Discovery*; Witty, D. R., Cox, B., Eds.; Prog. Med. Chem.; Elsevier, 2019; Vol. 58; pp 1 – 62.
- (12) Yang, H.; Yang, M.; Ding, Y.; Liu, Y.; Lou, Z.; Zhou, Z.; Sun, L.; Mo, L.; Ye, S.; Pang, H.; Gao, G. F.; Anand, K.; Bartlam, M.; Hilgenfeld, R.; Rao, Z. The Crystal Structures of Severe Acute Respiratory Syndrome Virus Main Protease and Its Complex with an Inhibitor. *Proc. Natl. Acad. Sci. USA* **2003**, *100*, 13190–13195.
- (13) Jacobs, J.; Zhou, S.; Dawson, E.; Daniels, J. S.; Hodder, P.; Tokars, V.; Mesecar, A.; Lindsley, C. W.; ; Stauffer., S. R. Discovery of Non-Covalent Inhibitors of the SARS Main Proteinase 3CLpro. *Probe Reports from the NIH Molecular Libraries Program* **2010**, <https://www.ncbi.nlm.nih.gov/books/NBK133447/>.
- (14) Jacobs, J.; Grum-Tokars, V.; Zhou, Y.; Turlington, M.; Saldanha, S. A.; Chase, P.; Egger, A.; Dawson, E. S.; Baez-Santos, Y. M.; Tomar, S.; Mielech, A. M.; Baker, S. C.; Lindsley, C. W.; Hodder, P.; Mesecar, A.; Stauffer, S. R. Discovery, Synthesis, and Structure-Based Optimization of a Series of N-(tert-Butyl)-2-(N-arylamido)-2-(pyridin-3-yl) Acetamides (ML188) as Potent Noncovalent Small Molecule Inhibitors of the Severe Acute Respiratory Syndrome Coronavirus (SARS-CoV) 3CL Protease. *J. Med. Chem.* **2013**, *56*, 534–546.
- (15) Liu, X.; Zhang, B.; Jin, Z.; Yang, H.; Rao, Z. The Crystal Structure of 2019-nCoV Main Protease in Complex with an Inhibitor N3. RSCB PDB, pdbode: 6LU7.
- (16) Hu, T.; Zhang, Y.; Li, L.; Wang, K.; Chen, S.; Chen, J.; Ding, J.; Jiang, H.; Shen, X. Two Adjacent Mutations on the Dimer Interface of SARS Coronavirus 3C-like Protease Cause Different Conformational Changes in Crystal Structure. *Virology* **2009**, *388*, 324 – 334.

- (17) PlayMolecule™, <https://www.acellera.com>, accessed 20 February 2020.
- (18) Skalic, M.; Sabbadin, D.; Sattarov, B.; Sciabola, S.; De Fabritiis, G. From Target to Drug: Generative Modeling for the Multimodal Structure-Based Ligand Design. *Mol. Pharm.* **2019**, *16*, 4282–4291.
- (19) Morris, G. M.; Huey, R.; Lindstrom, W.; Sanner, M. F.; Belew, R. K.; Goodsell, D. S.; Olson, A. J. AutoDock4 and AutoDockTools4: Automated Docking with Selective Receptor Flexibility. *J. Comput. Chem.* **2009**, *30*, 2785–2791.
- (20) O’Boyle, N. M.; Banck, M.; James, C. A.; Morley, C.; Vandermeersch, T.; Hutchison, G. R. Open Babel: An Open Chemical Toolbox. *J. Cheminf.* **2011**, *3*, 33.
- (21) Cheng, T.; Zhao, Y.; Li, X.; Lin, F.; Xu, Y.; Zhang, X.; Li, Y.; Wang, R.; Lai, L. Computation of Octanol-Water Partition Coefficients by Guiding an Additive Model with Knowledge. *J. Chem. Inf. Model.* **2007**, *47*, 2140–2148.
- (22) Graziano, V.; McGrath, W. J.; Yang, L.; Mangel, W. F. SARS CoV Main Proteinase: The Monomer-Dimer Equilibrium Dissociation Constant. *Biochemistry* **2006**, *45*, 14632–14641.
- (23) Kim, S.; Thiessen, P. A.; Bolton, E. E.; Chen, J.; Fu, G.; Gindulyte, A.; Han, L.; He, J.; He, S.; Shoemaker, B. A.; Wang, J.; Yu, B.; Zhang, J.; Bryant, S. H. PubChem Substance and Compound Databases. *Nucleic Acids Res.* **2016**, *44*, D1202–D1213.
- (2) Pronk, S.; Páll, S.; Schulz, R.; Larsson, P.; Bjelkmar, P.; Apostolov, R.; Shirts, M. R.; Smith, J. C.; Kasson, P. M.; van der Spoel, D.; Hess, B.; Lindahl, E. GROMACS 4.5: a High-Throughput and Highly Parallel Open Source Molecular Simulation Toolkit. *Bioinformatics* **2013**, *29*, 845.
- (3) Van Der Spoel, D.; Lindahl, E.; Hess, B.; Groenhof, G.; Mark, A. E.; Berendsen, H. J. C. GROMACS: Fast, Flexible, and Free. *J. Comput. Chem.* **2005**, *26*, 1701–1718.

- (26) Macchiagodena, M.; Pagliai, M.; Andreini, C.; Rosato, A.; Procacci, P. Upgrading and Validation of the AMBER Force Field for Histidine and Cysteine Zinc(II)-Binding Residues in Sites with Four Protein Ligands. *J. Chem. Inf. Model.* **2019**, *59*, 3803–3816.
- (27) Procacci, P.; Chelli, R. Statistical Mechanics of Ligand-Receptor Noncovalent Association, Revisited: Binding Site and Standard State Volumes in Modern Alchemical Theories. *J. Chem. Theory Comput.* **2017**, *13*, 1924–1933.
- (28) Gilson, M. K.; Given, J. A.; Bush, B. L.; McCammon, J. A. The Statistical-Thermodynamic Basis for Computation of Binding Affinities: A Critical Review. *Biophys. J.* **1997**, *72*, 1047–1069.
- (29) Nerattini, F.; Chelli, R.; Procacci, P. II. Dissociation Free Energies in Drug- $\alpha$ -Receptor Systems Via Nonequilibrium Alchemical Simulations: Application to the FK506-Related Immunophilin Ligands. *Phys. Chem. Chem. Phys.* **2016**, *18*, 15005–15018.
- (30) Procacci, P. I. Dissociation Free Energies of Drug-Receptor Systems Via Nonequilibrium Alchemical Simulations: a Theoretical Framework. *Phys. Chem. Chem. Phys.* **2016**, *18*, 14991–15004.
- (31) Shirts, M. R.; Mobley, D. L. An Introduction to Best Practices in Free Energy Calculations. *Methods Mol. Biol.* **2013**, *924*, 271–311.

Supporting Information for “Inhibition of the Main Protease 3CL<sup>pro</sup> of the Coronavirus Disease 19 via Structure-Based Ligand Design and Molecular Modeling”

Table S1: SMILES code and labeling used in the paper for ligands obtained using LIGGAN.

SMILES	Comp.	logP	H <sub>acc</sub>	H <sub>don</sub>	n <sub>rot</sub>	ΔG (kcal/mol)			
						SARS-CoV-2		SARS-CoV	
						H-CYS	H-HID	H-CYS	H-HID
<chem>NC(=O)c1csc(CNCC(N)C(F)(F)F)c1</chem>	1	0.120	3	1	5	-5.46	-5.68	-6.83	-6.52
<chem>CCC(C(=O)NC(CC(C)C)C(=O)O)(C(=O)c1ccccc1)C(C)C</chem>	2	4.450	2	4	11	-6.64	-6.49	-6.15	-6.68
<chem>COCCc1ccc(Oc2ccc(Nc3nc(C)cc(C)n3)cc2)cc1</chem>	3	4.520	1	2	7	-7.56	-7.55	-7.01	-6.80
<chem>CCc1cc(=O)oc2ccc(-c3ccc4c3CCOC4)cc12</chem>	4	2.870	0	1	2	-6.34	-7.70	-6.46	-6.69
<chem>CCOC(=O)C(NC(=O)Cc1c[nH]c2cccc(C)c12)C(C)(C)C</chem>	5	3.670	1	2	8	-6.35	-6.99	-6.30	-6.24
<chem>COCCn1ccc2c(C(=O)Nc3ccc4c(c3)nnn4C)cccc21</chem>	6	1.810	1	3	6	-7.32	-6.76	-6.67	-6.43
<chem>COc1cccc(-c2cc(O)cc(F)n2)c1</chem>	7	2.560	1	2	3	-5.10	-5.22	-5.61	-5.21
<chem>CCN(CCC1CC1)C(=O)C1CCCN(CCNC(C)=O)C1</chem>	8	1.370	1	2	10	-6.46	-6.19	-6.07	-6.26
<chem>CCOC(=O)c1c(NCc2c[nH]nc2C)sc(CC)c1-c1ccc(F)cc1</chem>	9	5.440	1	2	8	-7.95	-6.51	-7.43	-7.11
<chem>CC(C)N1CC(c2ncc(-c3cc(Br)c[nH]c3=O)[nH]2)CC1=O</chem>	10	2.150	0	3	3	-6.74	-6.74	-5.74	-5.98
<chem>CCC(NC(=O)Cc1c(C)[nH]c2cccc12)C(CC)S(=O)(=O)C1CC1</chem>	11	3.510	1	3	9	-7.20	-7.38	-7.03	-7.03
<chem>CC(C)(C)C(C)(C)CCNC(=S)NCC(N)=O</chem>	12	2.540	3	1	9	-6.27	-5.77	-5.66	-5.73
<chem>Cc1cc(F)cc2[nH]c(C(=O)Nc3ccc(C(=O)OC(C)(C)C)c3)cc12</chem>	13	3.450	1	3	6	-6.84	-7.62	-7.07	-6.51
<chem>O=C(Nc1ccc2ccc2c1)c1sc2cc(C(F)(F)F)ccc2c1F</chem>	14	5.500	1	1	3	-6.13	-6.32	-5.53	-5.19
<chem>CC(=O)C(NC(=O)c1cnc2c(c1)c(=O)[nH]c(=O)n2C1CC1)C(C)C</chem>	15	3.020	1	5	6	-6.37	-6.61	-5.95	-6.04
<chem>COCC(C)CC(=O)Nc1ncc(Cc2cc(F)cc(F)c2)s1</chem>	16	3.200	1	2	8	-6.74	-6.13	-7.07	-7.03
<chem>COCCn1cc(C(=O)N=c2[nH][nH]c(C)c2-c2ccc(F)cc2)cn1</chem>	17	3.380	0	2	6	-6.68	-6.90	-6.84	-7.03
<chem>COc1ccc(-c2cccc3c2COC3=O)cc1</chem>	18	2.940	0	1	2	-5.73	-5.68	-5.20	-5.19
<chem>CCC(=O)c1cc(C(=O)N=c2nc(-c3ccc(OC)cc3)[nH]s2)ccc1F</chem>	19	5.580	0	3	6	-8.03	-8.26	-7.01	-7.12
<chem>CCc1ccc(NC(=O)c2ccc3ccc3c2)cc1F</chem>	20	4.900	1	1	4	-7.23	-6.10	-5.31	-5.46
<chem>COc1ccc(Oc2nccn2)cc1OC</chem>	21	2.010	0	2	4	-5.74	-5.56	-4.86	-4.96
<chem>COCCOc1ccc(NC(=O)c2sc(-c3cnn(C)c3)nc2C)cc1</chem>	22	2.320	1	3	8	-6.91	-7.19	-6.51	-6.39
<chem>CCC(c1ccc(F)cc1)c1nc(-c2ccc(CNC)cc2)no1</chem>	23	3.910	1	2	6	-7.02	-7.09	-7.86	-7.55
<chem>CCOC(=O)COc1ccc(NC(=O)c2c[nH]cc2C)cc1C1</chem>	24	2.800	1	2	8	-7.63	-7.23	-7.43	-7.59
<chem>COc1cc2c(cc1F)oc1ccc(OCC(F)F)cc12</chem>	25	4.560	0	0	4	-5.98	-5.61	-5.26	-5.16
<chem>COCC(=O)Nc1cccc(-c2cnn(Cc3nc(C)cs3)c2)c1F</chem>	26	2.080	1	3	7	-6.57	-6.45	-6.47	-6.07
<chem>COCCOc1cc(C(=O)N=c2[nH][nH]c(C)c2-c2ccc(Cl)cc2)ccn1</chem>	27	4.900	0	2	7	-8.92	-8.79	-8.92	-9.46
<chem>CC(=O)NCCN(CC1CCCC1)CC1CCOC1</chem>	28	2.550	1	1	8	-6.89	-6.72	-5.88	-5.52
<chem>CC(C(=O)N1CC2CCC12C(=O)O)=C1C(=O)c2cccc2SC1=S</chem>	29	2.730	1	4	4	-6.61	-6.07	-6.44	-6.69
<chem>CCOC(=O)c1cnc2nc(C)ccc2c1Nc1ccc(CCO)cc1</chem>	30	3.740	2	4	8	-8.84	-8.19	-7.47	-7.86
<chem>COCC(=O)Nc1ccc(-c2noc(-c3ncc(Cl)c3)n2)cc1</chem>	31	2.080	1	4	6	-7.55	-7.51	-7.94	-6.80
<chem>COCCc1ccc1-c1nc2cc(F)ccc2o1</chem>	32	2.280	0	1	3	-5.29	-5.27	-5.06	-4.97
<chem>COCCc1ccc2cc(Nc3nnc(-c4cnn(C)c4)n3C)ccc2c1</chem>	33	2.640	1	3	6	-6.94	-7.08	-7.06	-6.93
<chem>COC(=O)CC(NC(=O)c1c[nH]cc1-c1cnn(C)c1)c1cccnc1</chem>	34	0.210	1	4	8	-6.80	-7.42	-5.95	-6.85
<chem>COc1cccc(-c2nc3cccnc3s2)c1F</chem>	35	3.380	0	2	2	-5.60	-5.72	-4.89	-4.85
<chem>CCOC(=O)C(CC)(CC)CNC(=O)C(c1ccccc1)C1CC1</chem>	36	4.120	1	2	11	-7.14	-6.45	-6.54	-7.02
<chem>COc1cc(-c2ccc3nsnc23)sn1</chem>	37	2.820	0	3	2	-5.93	-5.97	-5.89	-5.73
<chem>Cc1[nH]c2cccc2c(=O)c1CC(=O)N(CC(=O)OC(C)(C)C)C(C)C</chem>	38	4.360	0	3	8	-7.64	-8.02	-7.60	-6.76
<chem>CCC(C)C(NC(=O)OC(C)(C)C)C(=O)N=c1[nH]sc2cccc12</chem>	39	6.060	1	2	8	-8.25	-7.08	-6.82	-6.72
<chem>COCCn1c(C)c(C)c2cc(NC(=O)c3c[nH]cc3-c3ccc(C)o3)ccc21</chem>	40	3.300	1	1	7	-7.19	-6.98	-7.04	-7.80

SMILES	Comp.	logP	H <sub>acc</sub>	H <sub>don</sub>	n <sub>rot</sub>	ΔG (kcal/mol)			
						SARS-CoV-2		SARS-CoV	
						H-CYS	H-HID	H-CYS	H-HID
CNCc1cccc(NC2CCCCNC2)c1	41	1.760	3	0	4	-6.09	-6.92	-6.94	-6.64
COc1ccsc1-c1cccc(C(=O)O)c(F)c1	42	2.860	1	2	4	-5.12	-5.17	-4.32	-4.40
CCc1cccc(-n2c(=O)[nH]c3ccc(OC(C)=O)cc3e2=O)c1	43	5.120	0	3	4	-6.57	-6.79	-6.52	-6.48
COc1ccc2c(c1)OCCO2	44	1.610	0	0	1	-4.45	-4.54	-4.00	-3.96
COCCOc1cccc1C(=O)N=c1cc(-c2cccc(F)c2F)[nH][nH]1	45	4.100	0	2	7	-6.70	-7.10	-6.51	-6.80
COC(=O)C(C)c1cccc(NC(=O)c2cnn(-c3ccccc3)c2)n1	46	1.320	1	5	7	-6.70	-6.43	-6.76	-6.90
COc1ccc(-c2csc2C(=O)O)cc1	47	2.730	1	2	4	-5.29	-5.35	-5.25	-5.05
CCCC(C(=O)O)N(Cc1ccc(-n2cncn2)c(F)c1)c1nn[nH]n1	48	2.140	1	7	9	-5.96	-5.39	-5.94	-5.61
CCOC(=O)c1nc(Cn2ccc(-c3ccc4ncccc4c3)c2N)no1	49	2.610	1	4	6	-7.68	-7.49	-7.84	-7.21
COc1cccc(-c2nc(O)cc(O)n2)c1	50	1.790	2	4	4	-5.72	-5.46	-6.02	-5.86
CCOC(=O)CCN(C(=O)c1[nH]c2cccc2c1Br)C(C)(C)C	51	3.710	0	2	8	-7.02	-6.84	-6.79	-6.65
CN(C)Cc1cccc(CN(C)C)c1	52	1.590	0	0	4	-4.59	-5.33	-5.32	-5.26
CCOC(=O)c1c[nH]c2c(NC3ccc(-n4ccnc4)nc3)ccnc12	53	1.780	1	4	7	-6.41	-7.01	-6.35	-6.16
CCc1nc2ccc(C(=O)Nc3ccc(C)cc3C)cc2s1	54	4.780	1	2	4	-6.46	-6.38	-6.60	-6.24
Ce1noc2nc(-c3ccc(F)cc3)cc(C(=O)NCCCCO)c12	55	2.440	2	4	8	-6.99	-7.57	-7.37	-6.84
CCC1(C(=O)N=c2nc[nH]c3cccc23)CCCN1C(=O)OC(C)(C)C	56	4.460	0	3	6	-6.96	-7.34	-7.45	-7.13
COc1cccc(-c2enc3ccc(F)cc3n2)c1	57	2.940	0	2	2	-6.05	-6.05	-5.15	-4.94
COc1cc(C(F)(F)F)ccc1-c1en2cccnc2n1	58	3.630	0	2	2	-5.49	-5.14	-4.75	-4.80
COCCN(CC1CCC1)CC1CCN(C2CC2)CC1	59	2.740	0	0	8	-6.66	-6.47	-5.55	-6.35
CC(C)CC(=O)Nc1c[nH]nc1-c1cc(-c2ccc(F)cc2)no1	60	2.560	1	3	6	-7.59	-7.92	-6.34	-6.72
COc1ccc(-c2cccc2OC)cc1	61	3.490	0	0	3	-5.20	-5.36	-5.23	-5.18
N=C(N)c1cccc(NC2CCCC2)c1	62	2.140	2	0	3	-5.71	-5.76	-5.54	-5.17
CCOC(=O)C(C)N1CC2CCCC(NCC(C)C)C2C1	63	3.050	1	1	7	-6.86	-7.35	-6.60	-6.50
CC(C)(C)OC(=O)Nc1cc(-c2nc(-c3c[nH]c(=O)[nH]3)co2)co1	64	2.510	1	3	6	-7.17	-7.10	-6.86	-7.27
COc1cc(-c2cccc3e2OCC3=O)ccc1O	65	2.720	1	2	3	-6.01	-6.58	-5.70	-6.21
NCc1cccc(NC2CCCC(O)C2)c1	66	1.410	3	1	4	-6.54	-6.74	-6.62	-7.30
CN1CCNC(c2cccc(CN)c2)C1=O	67	-0.350	2	1	2	-6.93	-6.82	-7.06	-6.66
CC(C(=O)Nc1ccc(C(C)(C)C)cc1)c1cccc1F	68	5.040	1	1	5	-6.68	-6.44	-5.88	-6.21
CCc1cccc1NC(=O)c1ccc(-c2nnc(C)o2)cc1	69	3.440	1	3	5	-6.77	-6.65	-6.53	-6.91
CC(C)(C)N1CCCC1C1CCN(C(=O)C2CC(N)C2)CC1	70	1.630	1	1	4	-6.30	-6.52	-6.92	-6.66
COCCn1c(-c2cccc(-n3cccn3)c2)nc2c(=O)[nH]c(=O)n(C)c2c1=O	71	3.360	0	5	5	-6.76	-6.78	-6.72	-6.77
COCCNc1nc(-c2nc(-c3ccc4ncccc4c3)no2)cs1	72	2.970	1	4	6	-7.60	-7.30	-6.58	-6.77
NC(=O)c1csc(CN2CCC(F)(F)CC2)c1	73	1.510	1	1	3	-5.67	-6.04	-5.17	-4.50
COC(=O)C(C)(C)N(C)CCC1CCN(C(C)C)CC1	74	2.710	0	1	7	-7.11	-6.98	-6.30	-5.87
C#Cc1cccc(N(C)C(=O)c2ccc(-n3ccnc3)cc2)c1	75	2.940	0	2	5	-6.45	-6.58	-5.98	-5.87
COc1cccc1-c1ccc(CO)c(C=O)c1	76	2.100	1	2	5	-6.38	-6.41	-6.71	-6.30
CCOC(=O)c1c(Cc2nc(-c3cccc(N)c3)no2)n[nH]c1C	77	2.030	1	4	6	-8.17	-7.25	-7.43	-7.21
NC(=O)COc1ccc(-c2nc(-c3ccn4ccnc34)no2)cc1	78	2.220	1	4	5	-7.52	-7.86	-7.33	-6.36
NCc1cccc(NC2(C(F)F)CC2)c1	79	1.990	2	0	4	-5.18	-5.38	-5.43	-5.57
COCCc1nc2cc(NC(=O)c3ccc4[nH]nnc4cc3C)ccc2o1	80	2.290	1	4	6	-8.01	-8.31	-7.60	-7.35
NCCNc1cccc(CN2CCC2=O)c1	81	-0.030	2	1	5	-6.29	-5.38	-5.82	-6.04
COCCn1ccc2cc(NC(=O)c3cnc4onc(C)c4c3)ccc21	82	2.070	1	3	6	-7.92	-7.76	-6.92	-7.11
CCC(=O)c1cc(C(=O)Nc2ccc(-c3cnc[nH]3)cc2)ccc1OC	83	2.680	1	3	7	-6.82	-7.60	-6.46	-6.19
COC(=O)C1=CCC(NC2CC(N)C23CCCCC3)C1	84	2.140	2	1	4	-7.39	-7.18	-6.64	-6.89
CCC(=O)c1ccc(C(=O)c2cc(C)n(-c3cccc(O)c3)c2C)ccc1F	85	4.360	1	3	6	-7.50	-7.42	-7.66	-7.38
CC(=O)CC(C)(C)CC(=O)NC(c1c[nH]c2cccc12)C(C)(C)C	86	3.700	1	2	8	-6.55	-6.79	-6.43	-7.08
COc1ccc(-c2cncn2)cc1OC	87	1.390	0	2	3	-4.83	-4.96	-4.34	-4.33
COCCc1nc(-c2cccc(OC)c2)no1	88	1.460	0	2	4	-5.73	-5.81	-5.29	-5.26
COCC1(C(=O)NCC2CCN(CC(F)(F)F)CC2)CCC1	89	2.470	1	1	8	-6.96	-6.39	-5.41	-5.65
COc1ccsc1-c1ccc2c(c1)CC(CO)O2	90	2.620	1	1	4	-5.87	-5.53	-5.44	-5.00
CN(C)Cc1cccc(N=C(N)NCCO)c1	91	-0.040	3	1	7	-5.46	-6.07	-5.82	-5.31
COCCOc1cc(Nc2ccc3c(C)nn(C)c3e2)ccc1O	92	2.980	2	2	7	-6.64	-6.82	-6.60	-6.17

SMILES	Comp.	logP	H <sub>acc</sub>	H <sub>don</sub>	n <sub>rot</sub>	ΔG (kcal/mol)			
						SARS-CoV-2		SARS-CoV	
						H-CYS	H-HID	H-CYS	H-HID
<chem>CS(=O)(=O)CC1CCCN(CC2CCCC2CN)C1</chem>	<b>93</b>	0.990	1	2	5	-6.86	-7.59	-6.88	-5.81

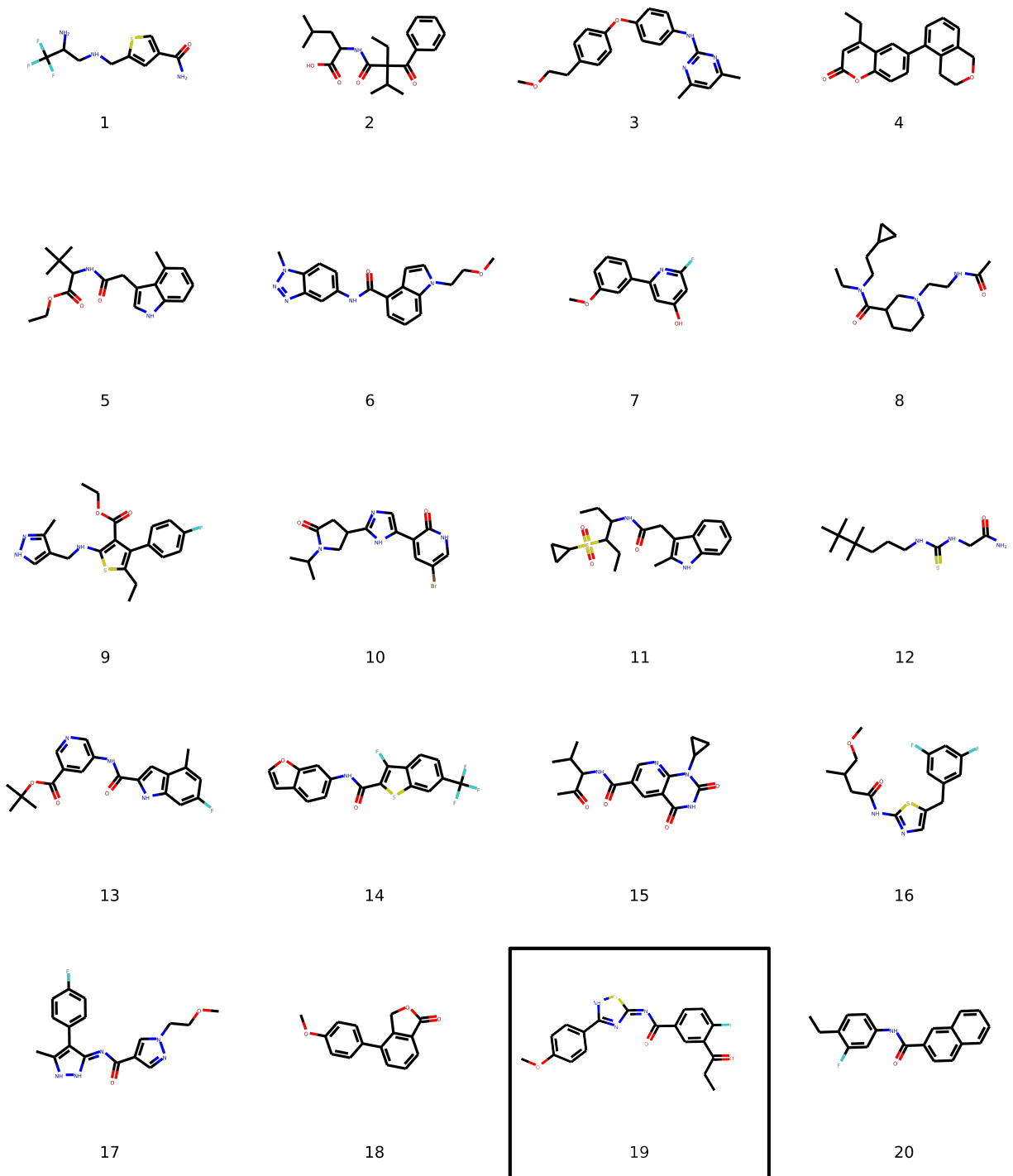


Figure S1: 2D-structures for compounds 1 to 20. In box one of the best five binders.

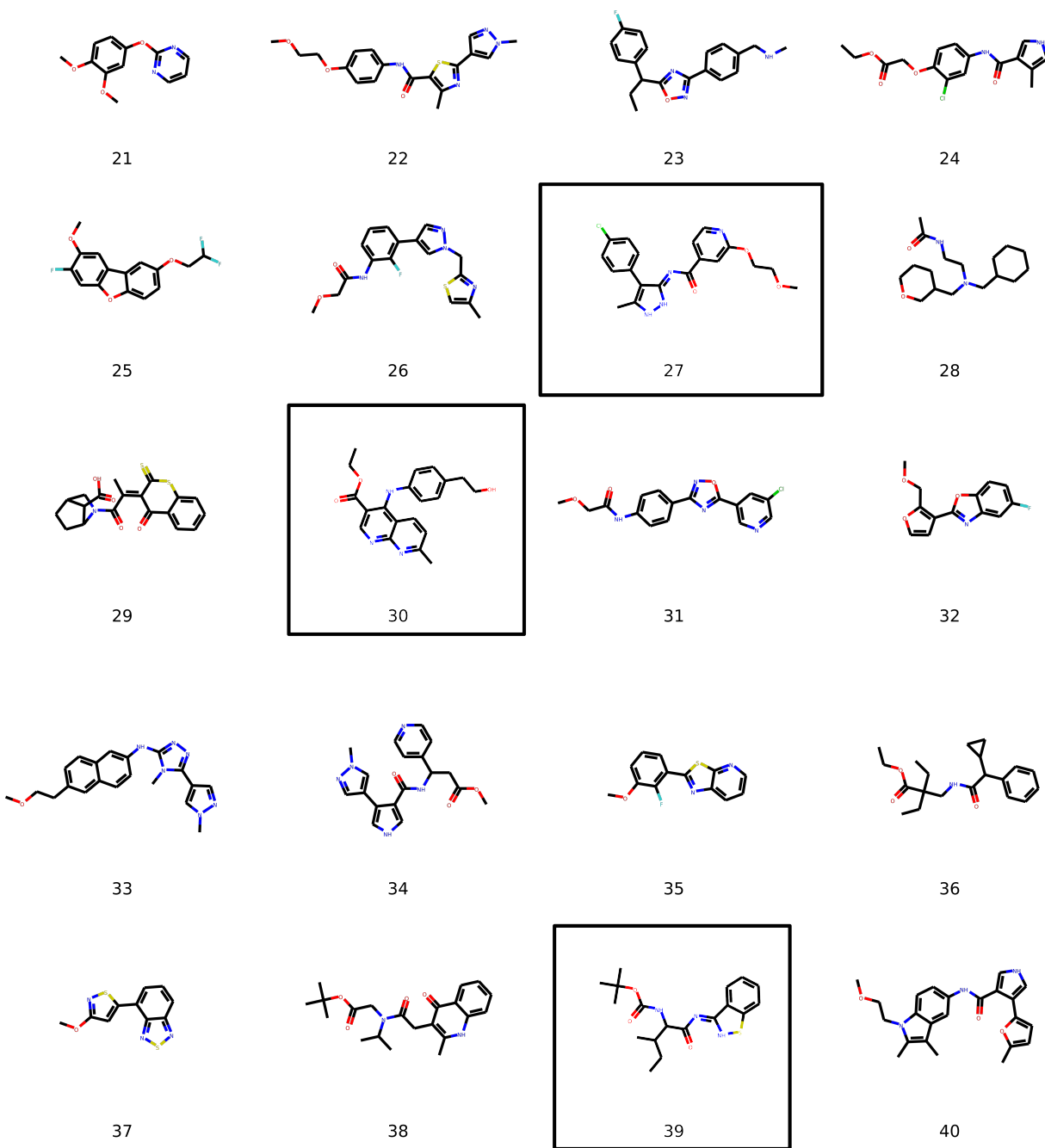


Figure S2: 2D-structures for compounds 21 to 40. In box three of the best five binders.

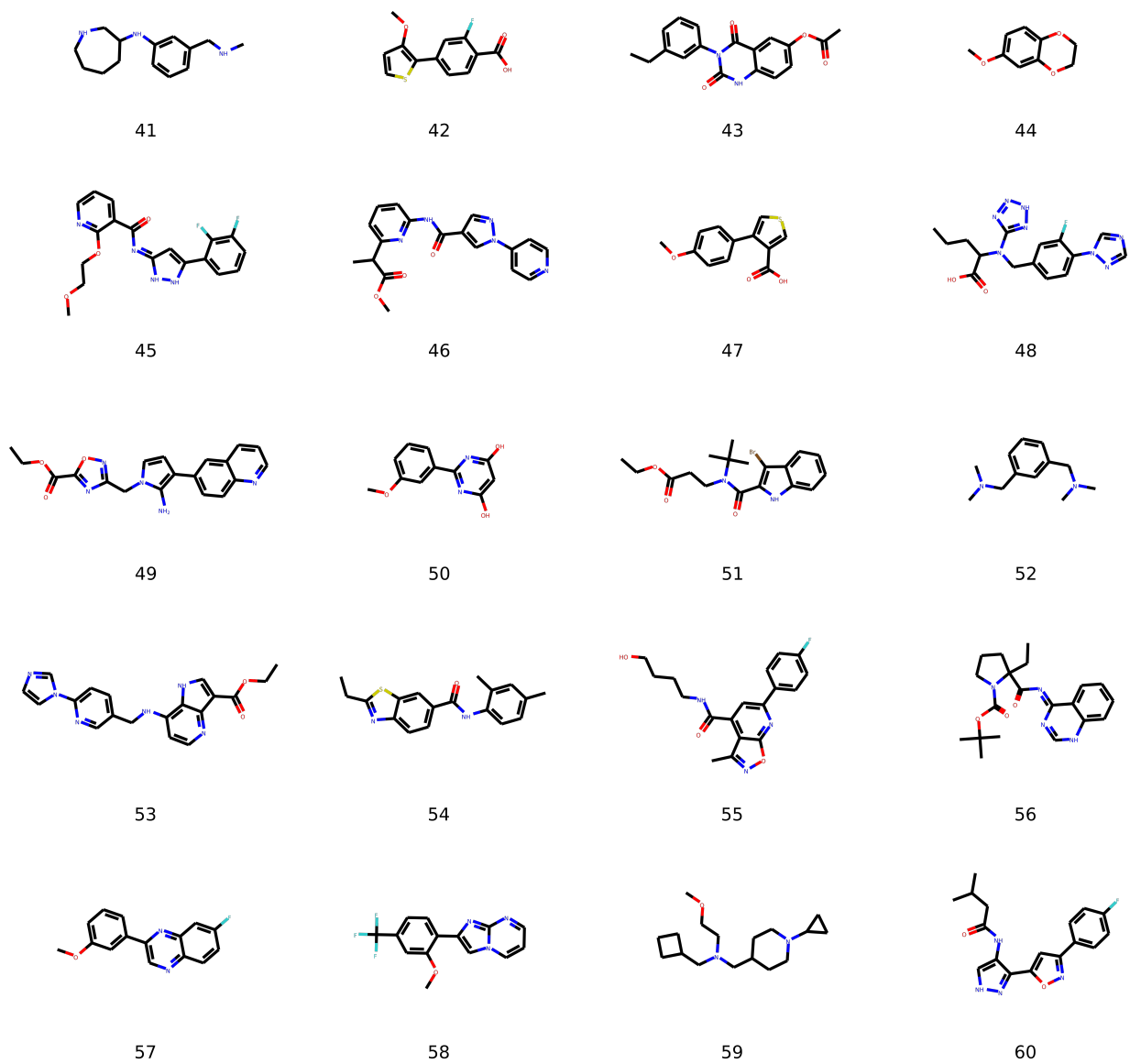


Figure S3: 2D-structures for compounds 41 to 60.

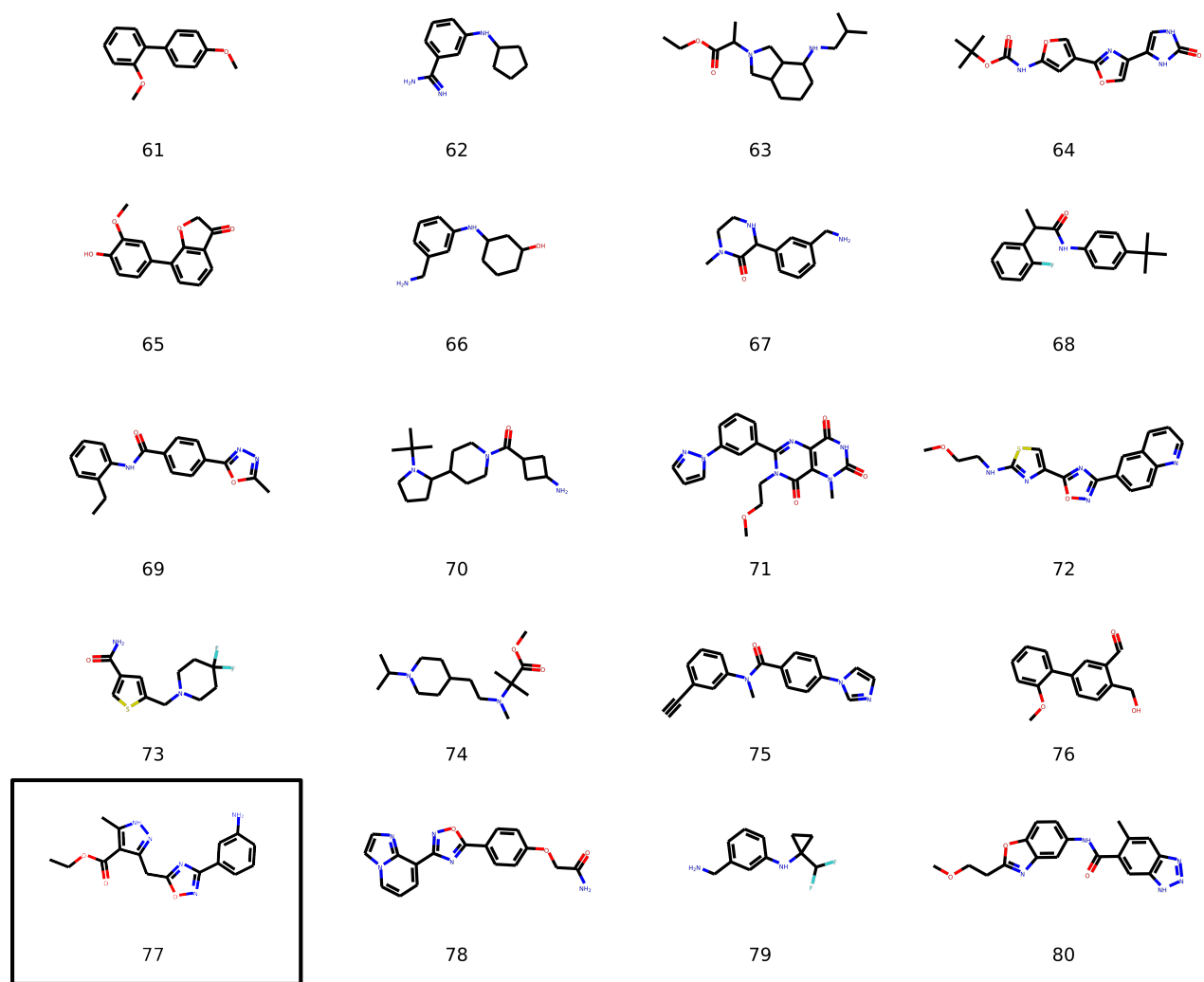


Figure S4: 2D-structures for compounds 61 to 80. In box one of the best five binders.

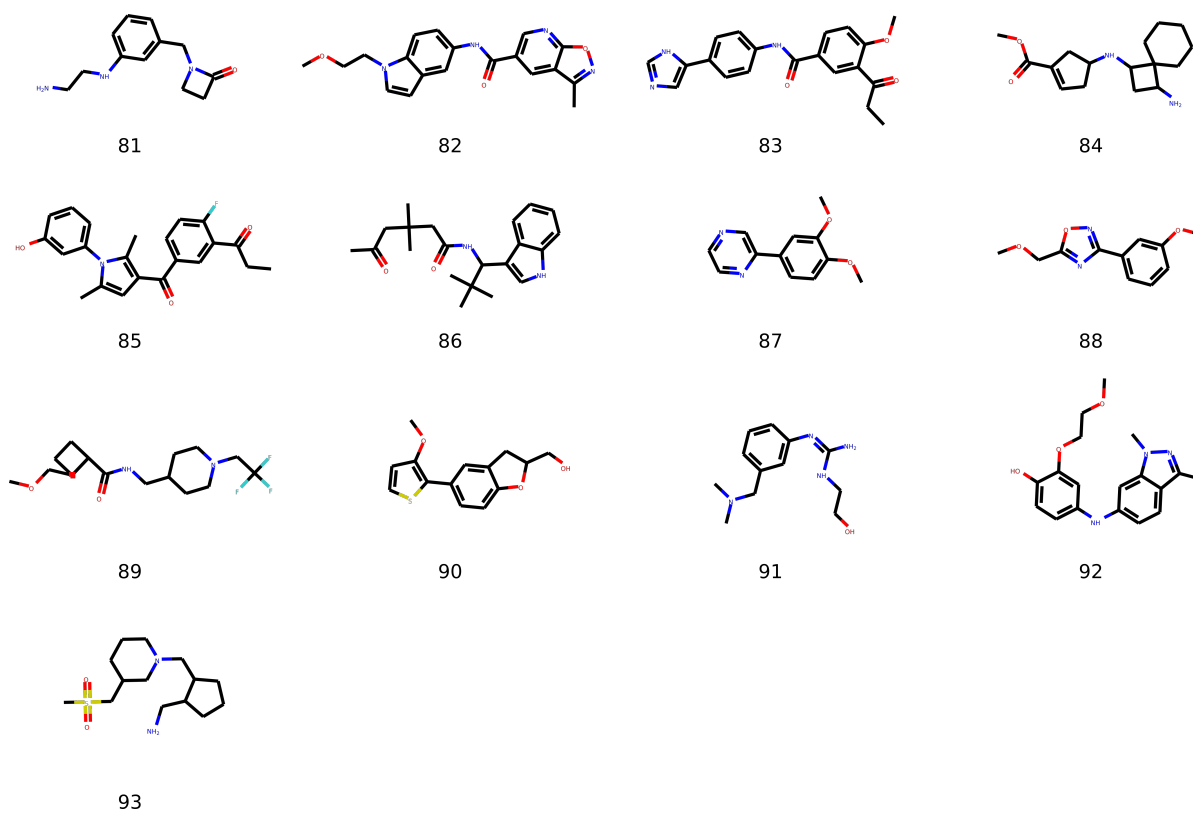


Figure S5: 2D-structures for compounds 81 to 93.

# Computational Details

## Molecular Docking

Following the two input file used for molecular docking.

- file.gpf

```
npts 60 60 60
gridfld 6lu7.maps.fld
spacing 0.375
receptor_types A C HD N OA SA
ligand_types ...
receptor 6lu7.pdbqt
gridcenter -10.18 20.65 66.75
smooth 0.5
map 6lu7.A.map
map ...
...
elecmap 6lu7.e.map
dsolvmap 6lu7.d.map
dielectric -0.1465
```

- file.dpf

```
autodock_parameter_version 4.2
outlev 1
intelec
seed pid time
ligand_types ....
```

```
fld 6lu7.maps.fld
map 6lu7.A.map
map ...
...
elecmap 6lu7.e.map
desolvmap 6lu7.d.map
move ligand.pdbqt
about 6.66645 -3.33598 -3.92332
tran0 random
quaternion0 random
dihe0 random
torsdof 4
rmstol 2.0
extnrg 1000.0
e0max 0.0 10000
ga_pop_size 150
ga_num_evals 2500000
ga_num_generations 27000
ga_elitism 1
ga_mutation_rate 0.02
ga_crossover_rate 0.8
ga_window_size 10
ga_cauchy_alpha 0.0
ga_cauchy_beta 1.0
set_ga
unbound_model bound
do_global_only 50
```

## Molecular Dynamics Simulations

Molecular dynamics (MD) simulations were carried out in a cubic box with periodic boundary conditions, whose side-length was chosen so that the minimum distance between protein atoms belonging to neighboring replicas was larger than 14 Å in any direction. The system (protein+compound) was explicitly solvated with the SPC/E<sup>1</sup> water model at the standard density. The starting configuration was generated using GROMACS<sup>2,3</sup> and PrimadORAC.<sup>4</sup> The system was initially minimized at 0 K with a steepest descent procedure and subsequently heated to 298.15 K in an NPT ensemble (P=1 atm) using Berendsen barostat<sup>5</sup> and velocity rescaling algorithm<sup>6</sup> with an integration time step of 0.1 fs and a coupling constant of 0.1 ps for 250 ps.

Production run in the NPT ensemble were carried out starting three independent simulations with different initial velocities randomization. Each MD run has been performed for 40 ns (for a total of 120 ns) imposing rigid constraints only on the X-H bonds (with X being any heavy atom) by means of the LINCS algorithm ( $\delta t=2.0$  fs).<sup>7</sup> Electrostatic interactions were treated by using particle-mesh Ewald (PME)<sup>8</sup> method with a grid spacing of 1.2 Å and a spline interpolation of order 4. The cross interactions for Lennard-Jones terms were calculated using the Lorentz-Berthelot<sup>9,10</sup> mixing rules and we excluded intramolecular non-bonded interactions between atom pairs separated up to two bonds. The non-bonded interactions between 1-4 atoms involved in a proper torsion were scaled by the standard AMBER fudge factors (0.8333 and 0.5 for the Coulomb and Lennard-Jones, respectively).

The simulations and the trajectories analysis were carried out using the GROMACS 2018.3 program.<sup>2,3</sup>

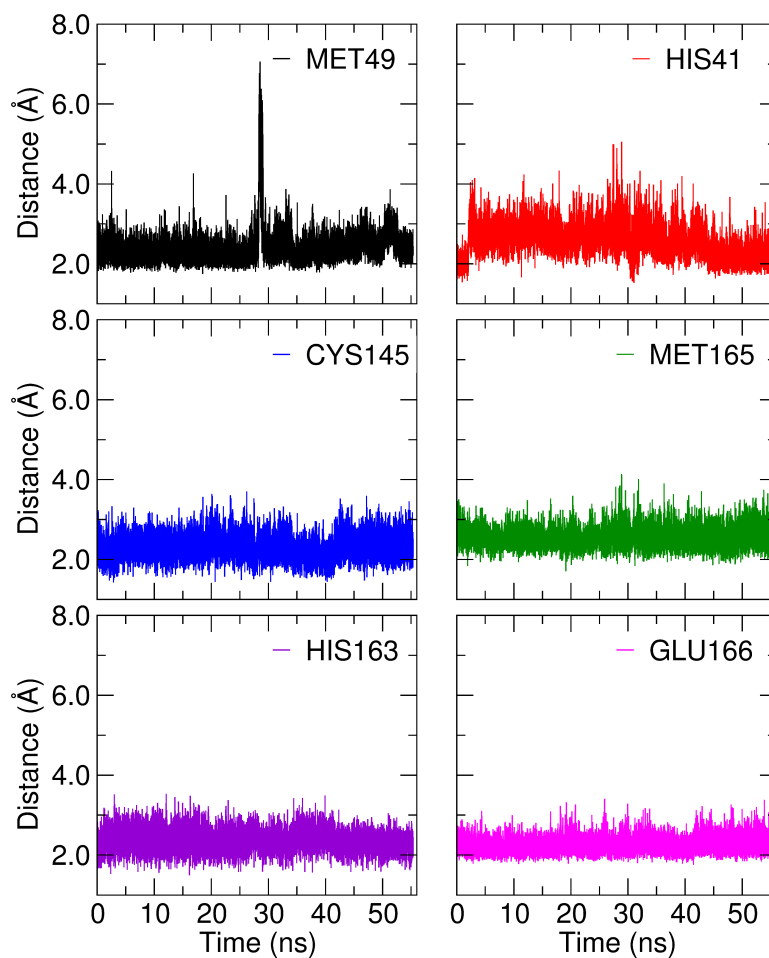


Figure S6: Pair distribution function between compound **27** and pocket residues (MET49, HIS41, CYS145, MET165, HIS163, GLU166), calculated during 55 ns of MD simulation.

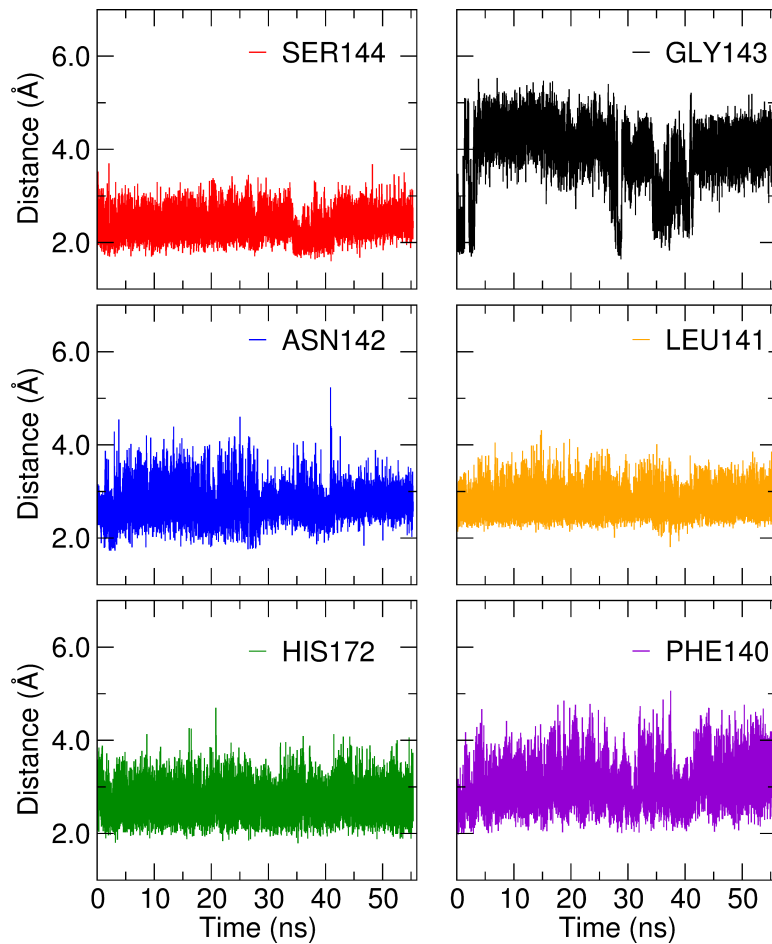


Figure S7: Pair distribution function between compound **27** and pocket residues (SER144, GLY143, ASN142, LEU141, HIS172, PHE140), calculated during 55 ns of MD simulation.

## References

- (1) Berendsen, H. J. C.; Grigera, J. R.; Straatsma, T. P. The Missing Term in Effective Pair Potentials. *J. Phys. Chem.* **1987**, *91*, 6269–6271.
- (2) Pronk, S.; Páll, S.; Schulz, R.; Larsson, P.; Bjelkmar, P.; Apostolov, R.; Shirts, M. R.; Smith, J. C.; Kasson, P. M.; van der Spoel, D.; Hess, B.; Lindahl, E. GROMACS 4.5: a High-Throughput and Highly Parallel Open Source Molecular Simulation Toolkit. *Bioinformatics* **2013**, *29*, 845.
- (3) Van Der Spoel, D.; Lindahl, E.; Hess, B.; Groenhof, G.; Mark, A. E.; Berendsen, H. J. C. GROMACS: Fast, Flexible, and Free. *J. Comput. Chem.* **2005**, *26*, 1701–1718.
- (4) Procacci, P. PrimaDORAC: A Free Web Interface for the Assignment of Partial Charges, Chemical Topology, and Bonded Parameters in Organic or Drug Molecules. *J. Chem. Inf. Model.* **2017**, *57*, 1240–1245.
- (5) Berendsen, H. J. C.; Postma, J. P. M.; van Gunsteren, W. F.; Di Nola, A.; Haak, J. R. Molecular Dynamics with Coupling to an External Bath. *J. Chem. Phys.* **1984**, *81*, 3684–3690.
- (6) Bussi, G.; Donadio, D.; Parrinello, M. Canonical Sampling Through Velocity Rescaling. *J. Chem. Phys.* **2007**, *126*, 014101.
- (7) Hess, B.; Bekker, H.; Berendsen, H.; Fraaije, J. LINCS: A Linear Constraint Solver for Molecular Simulations. *J. Comput. Chem.* **1997**, *18*, 1463–1472.
- (8) Darden, T.; York, D.; Pedersen, L. Particle Mesh Ewald: An  $N \log(N)$  Method for Ewald Sums in Large Systems. *J. Chem. Phys.* **1993**, *98*, 10089–10092.
- (9) Antoon, L. H. Ueber die Anwendung des Satzes vom Virial in der Kinetischen Theorie der Gase. *Ann. Phys* **1881**, *248*, 127–136.

- (10) Marcellin, B. Sur Le M<sup>̃</sup>llange Des Gaz. *Comptes Rendus Acad. Sci.* **1898**, *126*, 1703–1855.